VERTICAL AND SLOPED BANK EFFECTS ON DIFFERENT SHIP TYPES

(DOI No: 10.3940/rina.ijme.2015.a3.340)

Dong-Taur Su, Department of Shipping Technology, National Kaohsiung Marine University, Kaohsiung, Taiwan

SUMMARY

This study employed computer design software to completely draft 3D ship models; then, computational fluid dynamics were used to establish numeric navigation channels and simulate fluid hydrodynamic analysis of ships navigating along shore banks. The parameters considered comprised bank type (vertical and sloped), ship model (two types), velocity, ship-to-bank distance, and navigation time. Figures and tables were used to present the distribution of ship stern eddy current, flow field pressure, and velocity, and the comparison of center of mass deviation, sway force, and yaw moment. Results showed that ships navigating along embankments and channels produced asymmetric flows, which draw the bow away from the shore. Larger ships are substantially more influenced by bank effects than smaller ships. Large sway forces and yaw moments are produced in large ships, drifting the bow away from the bank and the stern towards the bank, increasing the risk of collision with the embankment. From the study results, the characteristics of bank effects are understood and can be used for assisting the safe navigation of ships in restricted waters.

1. INTRODUCTION

Ships navigating in narrow channels are influenced by restricted boundaries such as the influence of ship–ship and ship–bank interactions. Asymmetric flows are produced in the ship navigation zones interfering with the stability of ship navigation directions, and bank suction and cushion substantially affect ship control, influencing ship navigation safety. According to the mariners' Standards of Training, Certification, and Watchkeeping (STCW 2010) from the 26th International Towing Tank Conference (ITTC) [1], mariners at the management level must be able to immediately handle emergency conditions and appropriately control ships; thus, bank effects are worthy of in-depth investigation. Bank effects are caused when the water flow between a ship and a bank increases, which causes the formation of a low pressure zone. Meanwhile, the inward suction and outward flow of water around the propeller blade surface facing the shore are not sufficient for replenishing the displaced water on time; therefore, water level decreases and pressure becomes lower than that in the outboard, drawing the ship stern toward the bank and producing a suction phenomenon, resulting in bank suction. Additionally, when ships advance, water flow is displaced toward the two sides of the ship. The shore side is obstructed by the bank where water cannot diffuse, forming a higher water level. By contrast, water diffuses faster on the opposite side, forming a lower water level, which results in an outward deviation of the bow, which is called bank cushion. Bank suction and bank cushion are collectively called bank effects. Ship velocity and ship-to-bank distance (distance to bank, BS) are the primary factors influencing the bank effects (Lo et al. [2]). When ships navigate along a bank, a vertical or sloped embankment will influence the magnitude of bank effects on a ship. In addition, ship size and tonnage will also directly influence bank effects.

This study investigated various types and sizes of ships navigating along vertical or sloped banks to explore and discuss the influences of the bank effects. A ship operator must understand the interaction between ship and shore to properly control ships. When a ship navigates along a bank, the hull is close to the bank, and the bank side of the midship and stern has a small cross-sectional flow area, which increases the water flow rate and reduces pressure; consequently, a pressure difference forms between the two sides of the ship, pushing the ship toward the shore. This lateral suction force is called bank suction. If the ship deviates toward one side of the channel in close proximity to the bank, the obstruction of the bank to the side of the ship decelerates the discharge and diffusion effect of water; subsequently, the hydrodynamics beneath the ship bottom are retarded because of the squat effect. Thus, high water levels form at the bow side near the bank, producing yaw moment that pushes the bow toward the center of the channel. This phenomenon is called bank cushion. Regarding factors that influence bank effects, model and actual ship experiments have been conducted to demonstrate that bank effects are related to the following factors: Strong bank effects are produced when (1) a ship is close to the shore and far off-course from the center of the channel, (2) the channel is narrow, (3) the ship is traveling at a high speed, (4) the ship hull is corpulent, (5) the ship has a large tonnage, and (6) the water depth is shallow.

In general, by studying ship hydrodynamics in confined waters, the relationship between a ship and a bank can be analyzed. When two ships are within a specific distance, the movements of the two ships interact; the operation of both ships will be influenced during fronting and passing. Ship models and experimental towing tanks can be used to simulate relevant ship motions. Norrbin [3] conducted experimental studies on the bank effects in 1974 and discovered that banks critically influence fluid dynamic coefficients. Ch'ng [4] and Ch'ng and Renilson [5] have studied the effect that varying bank effect factors such as ship type, water depth, ship speed, bank slope, and propeller speed had on the operability of the ships. High dependencies were found on the degree and direction of sway force and yaw moment produced when the depth to

draft ratios were below 1.5 ($h/T < 1.5$). Li et al. [6] used three types of ship models to conduct bank effect experiments, and the results indicated that the critical h/T ratio was approximately 1.10. When the h/T was nearly or below 1.10, the sway force changed from bank suction to bank cushion, and sway force and yaw moment substantially increased as a result of water depth reduction. This phenomenon conforms to Bernoulli's principle, which states that when a fluid flows from broad to narrow zones, velocity increases and pressure decreases, and vice versa. Pedersen[7] conducted review and application of ship collision and grounding analysis procedures. Lo et al.[2] used the bank effects on a simulated ship navigating along a vertical bank as a basis for extending this effect on the study of two ships during fronting and passing (Lo[8]). Parameters such as ship speed, ship distance, and navigation time were investigated. Ship speed and distance were demonstrated to influence the sway force and yaw moment of the ships. Zhou et al. [9] performs a series of simulations using computational fluid dynamics (CFD) software to examine the effects of a ship sailing along a bank in restricted waters. Ma et al. [10] discussed the vessel speed and distance to bank on the magnitude and time-based variation of the hydrodynamic interaction among hull, rudder and bank for a ship sailing along a bank in restricted waters.

Along with the enhancement of the computational power of computers, computational fluid dynamics (CFD) has reached incredible precision and reliability in numerical simulations of fluid structure-coupled problem bodies. Regarding ship towing tests, CFD technology can directly perform numerical simulation and visualization postprocessing, present coupled motion of the hull with 6 degrees of freedom (DOFs), compute physical values such as velocity field vectors, pressures, and vorticity distributions in the computation zone. Thus, ship–bank interactions can be observed, and the physical phenomena of the flow field can be further analyzed. To save time and financial costs necessary for conducting tank experiments, and to visualize physical values such as velocity and pressure field distributions around a ship on a computer (values that are difficult to obtain in physical experiments), this study applied CFD for simulating the influences of bank effects on ships.

2. THEORETICAL AND NUMERICAL MODELS

This study adopted numerical methods to simulate the navigation of ships along banks and the bank effects produced. The simulation comprised vertical and sloped banks and how these influenced two types of ships. Computations were performed to solve the Navier–Stokes equations formula of the 3D viscous flow field to construct and analyze the models in this study. Regarding numerical methods, this study adopted the Finite difference method (FDM) for solving the time-dependent variation of flow field velocities and pressures. The techniques implemented in this study were adopted from several crucial fluid dynamic methods developed by Dr. C. W. Hirt from the Los Alamos National Laboratory in 1963, such as orthogonal grid systems for processing uneven boundaries and the original creation of the volume of fluid (VOF) free surface tracking technology. Dr. Hirt established Flow Science Inc. in 1980, published the VOF method for the dynamics of free boundaries with Hirt and Nichols[11] in 1981, and released the numerical analysis software for engineering and science simulations and industrial casting and mold flow analyses, in 1985. The unique fractional volume computation technology can provide extremely realistic and detailed free surface capture such as wave–structural object interactions and breaking wave simulations. A new-generation, high-precision fluid dynamic model was also developed and widely applied in the field of science and engineering for mold casting, reservoir hydrography, ocean outfall, and pollution dispersion analyses. Regarding maritime transport, the swaying of cargo in oil tankers, ship-wave coupled motions, bank effects, and interactions during ship fronting and passing can be analyzed.

Hull motion has 6 DOFs, comprising surging (displacement along the x-axis), broadsiding (displacement along the y-axis), heaving (displacement along the z-axis), rolling (rotation around the x-axis), pitching (rotation around the y-axis), and yawing (rotation around the z-axis) of the ship model's center of mass.

2.1 GOVERNING EQUATIONS

The partial differential equations governing the viscous and incompressible flow for the fluid medium are given by the Navier-Stokes equations. The corresponding dimensional form of the governing equations for conservation of mass and momentum can be expressed in x-, y- and z- axis coordinate system as:

Continuity equation

$$V_F \frac{\partial \rho}{\partial t} + \frac{\partial}{\partial x}\left(\rho u A_x\right) + \frac{\partial}{\partial y}\left(\rho v A_y\right) + \frac{\partial}{\partial z}\left(\rho w A_z\right) = R_{DIF} + R_{SOR} \tag{1}$$

Momentum equations

$$\frac{\partial u}{\partial t} + \frac{1}{V_F}\left\{uA_x \frac{\partial u}{\partial x} + vA_y \frac{\partial u}{\partial y} + wA_z \frac{\partial u}{\partial z}\right\} = -\frac{1}{\rho}\frac{\partial P}{\partial x} + G_x + f_x - b_x - \frac{R_{SOR}}{\rho V_F}\left(u - u_w - \delta u_s\right) \tag{2}$$

$$\frac{\partial v}{\partial t} + \frac{1}{V_F}\left\{uA_x \frac{\partial v}{\partial x} + vA_y \frac{\partial v}{\partial y} + wA_z \frac{\partial v}{\partial z}\right\} = -\frac{1}{\rho}\frac{\partial P}{\partial y} + G_y + f_y - b_y - \frac{R_{SOR}}{\rho V_F}\left(v - v_w - \delta v_s\right) \tag{3}$$

$$\frac{\partial w}{\partial t}+\frac{1}{V_F}\left\{uA_x\frac{\partial w}{\partial x}+vA_y\frac{\partial w}{\partial y}+wA_z\frac{\partial w}{\partial z}\right\}=-\frac{1}{\rho}\frac{\partial P}{\partial z}+ \\ +G_z+f_z-b_z-\frac{R_{SOR}}{\rho V_F}\left(w-w_w-\delta w_s\right) \tag{4}$$

Where V_F is the fractional volume open to flow, ρ and ν refer to the density and kinematic viscosity coefficients of the fluids respectively, R_{DIF} is a turbulent diffusion term, and R_{SOR} is a mass source. $V=(u,v,w)$ represent the instantaneous velocity components in the horizontal and vertical directions, (x,y,z) represent the respective coordinates in the horizontal and vertical directions. A_x is the fractional area open to flow in the x-direction, A_y and A_z are similar area fractions for flow in the y and z directions, respectively. P denotes the instantaneous pressure. These are maintained at set values without being influenced by other factors during the simulation process. (G_x, G_y, G_z) refer to the acceleration rate of the body, and (f_x, f_y, f_z) are the viscous accelerations terms, U_w = (u_w, v_w, w_w) are the velocity of the source component, which will generally be non-zero for a mass source at a general moving object, U_s = (u_s, v_s, w_s) are the velocity vectors of the fluid at the surface of the source relative to the source itself.

2.2 COUPLED SHIP MOTION EQUATIONS

This simulation primarily solves the coupled ship motion equations (Wei[12]). Two Cartesian coordinate systems were used to describe the body coordinate system and the space coordinate system, which are also called the body-fixed and earth-fixed systems (Baha[13]), respectively. In the following, the ship is defined as the body coordinate system. In contrast to numeric channel displacements, the (x, y, z) origin remained fixed in space and the coordinate axis sits parallel to the numeric channel axis when ship (x', y', z') t = 0. Ship movements consist of 6 DOFs. The ship origin is set at the center of mass G. The G point remained fixed relative to the ship, meaning that $u=v=w=\dot{u}=\dot{v}=\dot{w}=0$. The coordinate conversion between ship movement (x', y', z') relative to the numeric channel (x, y, z) is:

$$\vec{x}_s=[R]\cdot\vec{x}_b+\vec{x}_G \tag{5}$$

In the equation, $\vec{x}_s$ and $\vec{x}_b$ respectively represent the vectors of numeric channel and ship position; $\vec{x}_G$ is the positional vector of the numeric channel's center of mass; and $[R]$ represents the Cartesian conversion tensor.

According to kinematic theory, the general motions of rigid bodies can be divided into translational and rotational motions. When rotating around the origin, the velocity of an arbitrary point on the rigid body is identical to that of the chosen point of origin; thus, the center of mass of the object can be chosen as the origin of the 6 DOF motions. Let P be a point on the object with a velocity relative to the velocity $\vec{V}_G$ and angular velocity $\vec{\omega}$ of the center of mass:

$$\vec{V}_P=\vec{V}_G+\vec{\omega}\times\vec{r}_{P/G} \tag{6}$$

In the equation, $\vec{r}_{P/G}$ is the distance vector from G to P. On the right side of equation (6), the first and second terms represent the translational and rotational motions of the center of mass, respectively. Note that $\vec{\omega}$ is a property of a moving object and an independent choice of origin. The equation of motion rules the two separate motions:

$$\vec{F}=m\frac{d\vec{U}_G}{dt} \tag{7}$$

$$\vec{T}_G=[J]\cdot\frac{d\vec{\omega}}{dt}+\vec{\omega}\times\left([J]\cdot\vec{\omega}\right) \tag{8}$$

In the equations, G represents the center of mass, $\vec{F}$ is the total force, m is the mass of the rigid body, $\vec{T}_G$ is the total turning moment of G, $\vec{U}$ is the velocity of G, $\vec{\omega}$ is the angular velocity of G, and [J] is the moment of inertia tensor.

2.3 THREE-DIMENSIONAL SHIP MODELLING

Two 3D ship models were constructed in this study. Table 1 presents the geometric data of the two ship models. Ship 1 is a container ship and Ship 2 is a multipurpose ship. The ship models were drafted using the AutoCAD computer aided design (CAD) software. To construct the models, we established the ship type table: Table 1 presents the geometric parameters of the two types of ship models for inputting and drafting the ship models in AutoCAD. The origin (x = y = z = 0) was set at the node of the intersection line of the still water level and the midship cross-section and the vertical line of the ship stern. A total of 60 body plans were drafted from the ship stern toward the bow. Subsequently, we trimmed and converted the format of the model ship body: Ship models drafted by using AutoCAD, as shown in Figure 1, were exported to the numerical code-supported STereoLithography (STL) format. Then, the DA Design Expert meshing tool software was used to confirm the completeness of the STL object. Finally, the models were used to solve 3D Navier-Stokes equations.

3. RESULTS AND DISCUSSION

In the numerical simulated flow field computation example of this study, the fluid physical characteristic density and dynamic viscosity coefficient in the computation of the bank effect ship analysis were

$\rho = 1000\ kg/m^3$ and $\mu = 8.0 \times 10^{-4}\ kg/m \cdot \sec$, respectively; an average of 2,000,000 cells were used in each computation example.

3.1 SHIP RESISTANCE VERIFICATION

To confirm the accuracy of the models, the resistance of an Azimut yacht was calculated and compared with the experimental data. The geometric parameters of the Azimut yacht comprise a length of 3.0 m, a width of 0.8 m, a draft of 0.2 m, and a displacement of 118.2 kg. Assuming the yacht travels at 5.04, 5.88, 6.72, and 7.98 m/s in the open waters in increments of 8 s, the average resistances (from 4–8 s) of the yacht moving in the *x*-direction were obtained. Table 2 shows the results and comparisons with experimental values (Wei [14]) of this model. One of the aims of the present numerical scheme is to show that the use of two grids to achieve good solutions with the comparisons of the experimental results. This has great advantage while dealing with three-dimensional flow problems. In order to validate the computer program developed to solve the governing equations for a yacht travels at various speeds in the open waters, a total of 300,000 (Grid1) and 600,000 (Grid2) computational cells were used for testing a grid independence study in this model. The direct numerical simulation method was used in the numerical model, which also considered the viscosity effect. The 6-axis coupled motions of the yacht were solved using general moving objects.

3.2 INVESTIGATING THE BANK EFFECTS OF TWO DIFFERENT SHIP TYPES

This study used two types of ships: a container ship (Ship 1) and a multipurpose ship (Ship 2). Ship 1 was a 3,600 TEU container ship, with a ship length of 230 m, a width of 32.2 m, and a draft of 10.8 m. Detailed ship parameters were obtained from Lo et al.[2]. The multipurpose ship had a length of 171 m, a width of 27.6 m, and a draft of 8.4 m. The ship models used in this study were constructed using the 3D coordinates in a table of ship types. Based on these coordinates, parameters were input to the 3D CAD software to draft the ships. The node of the intersecting line of the still water level and the midship cross-section and the vertical line of the stern were designated as the point of origin. A total of 60 body plans were created from the ship stern to the bow. Figure 1 shows the 3D diagrams of the two ship types completed using the CAD software. Figure 2 illustrates the schematics of each parameter of the ship and the embankment; *B* is the ship width, and □ is the angle of embankment, which varied from 0° (vertical), 30°, to 60° (sloped) in this study. The BS is 0.5 and 1.0 times the width of the ship. The ship navigated in the direction parallel to the bank at a low navigation speed set at 3 kn (1.54 m/s).

This section presents the conditions of the position of the ships' centers of mass, sway force, yaw angular velocity, yaw moment, velocity field, and pressure field with the variation of time. Figure 3 (a) and (b) present the deviation of the ships' centers of mass when Ship 1 and Ship 2 navigated along embankments of various angles. Generally, a vertical bank caused a larger off-course deviation than sloped banks did, and Ship 1 caused a larger deviation than Ship 2 did because Ship 1 was larger and heavier than Ship 2. The *x*-axis in Figure 3 represents navigation time and the *y*-axis represents the distance of the ship's center of mass away from the embankment, which was quantified using the ship width (*B*). Figure 3 shows that despite a ship speed of 3 kn, a d2b of 0.5 *B* resulted in obvious bank suction with substantial ship deviation. By simulating the navigation of two ship types along the embankment with fixed d2b, the bank effects were obvious even at low navigation speeds. Figure 4 (a) and (b) present the conditions of Ship 1 and Ship 2 under sway force with respect to time. The figure shows that sway forces were smaller in vertical banks than in sloped banks and smaller in Ship 2 than in Ship 1. Identical trends in the change of sway force for the two sloped banks were observed, oscillating in decline. Under continuous bank suction on the ships' bows and sterns, the ships gradually drifted away from the bank; thus, when the ships evidently drifted from the bank, the bank effects on the ships gradually reduced.

The ships' motion consisted of 6 DOFs; when moving along the *x*-axis, the bow direction simultaneously swayed against the *z*-axis. According to the right-hand rule, a positive angular velocity represents a counterclockwise rotation around the *z*-axis, the bow points to the left and the course angle is reduced, and vice versa. As shown in Figure 5, the off-course deviation angular velocities were collectively positive, indicating counterclockwise rotations around the *z*-axis, therefore the bow points to the left and the course angle reduces. By comparing the conditions of the three bank angles, the angular velocities of Ships 1 and 2 increased in oscillation with time, revealing that the ships were continually influenced by the bank effects during navigation and that the off-course angular velocity gradually increased, which raises the difficulty of ship operation; thus, ship operators navigating along embankments must preemptively respond to bank effects and always maintain course stability and high alertness. Figure 6 illustrates the variation of yaw moment with respect to time. Ship 1 had a larger tonnage than Ship 2 did, thus it had more obvious yaw moments than those of Ship 2, regardless of vertical or sloped banks. Yaw moments oscillated between positive and negative values with time. Generally, ships experience larger yaw moments when navigating through vertical banks than through sloped banks; however, special attention must be paid to submerged portions of sloped banks because they are difficult to detect, which increases the risk of collisions. Taking the ship 2 along the embankment

with 0.5 B and 1.0 B as an example, Figure 7 shows the variance of center of mass deviating from the bank for verical and sloped bank. The simulation results clearly indicates that for a constant ship speed, the center of mass deviating from the bank increases as the distance between the ship and the verical or sloped bank.

According to the simulation results, the more obvious the eddy currents produced at the ship stern, the larger the bank effects on the ship. Figure 8 shows the eddy current phenomenon produced at the stern of Ship 1. When the ship navigated for 50 s, no eddy currents have yet produced at the ship stern; however, the effects of bank suction became increasingly obvious as navigation time increased. As seen in the figure, obvious eddy currents were produced (in a counterclockwise rotation) at t = 150 s. In the figure, the ship was influenced by the ship stern eddy current on the port side and its bow deviated towards the center of the navigating channel. Figures 9 and 10 are the pressure variations on the x-y plane 1 m below the surface of water for Ships 1 and 2, respectively, when navigating along a vertical embankment. Red represents high pressure zones and blue represents low pressure zones. The figures show that the area between the ship stern and the embankment was a low pressure zone; thus, as navigation time increased, the ship stern increasingly approached the embankment because of bank suction. The pressure waves at the bow moved forward, and the pressure on the starboard side became higher than that on the port side, producing a bank cushion effect and causing course deviation.

4. CONCLUSION

In this study, 3D physical modelling was applied to construct ship models and fluid dynamic computational methods were used to simulate two types of ships navigating in restricted waters for analyzing the induced bank effects. The simulation results revealed that the bank effects produced during the navigation of ships were influenced by the following factors: ship type, draft, under keel clearance, trim, list, navigation speed, water depth, channel geometry, distance to bank(BS), and wind pressure. This study only investigated two types of ships navigating at 3 kn along banks with a BS of 0.5 B and 1.0 B. Under such conditions, obvious bank effects were produced, both bank suction and bank cushion, during ship navigation in regular restricted waters. Intense bank effects were observed when the ship was close to the bank and far away from the center of the navigation channel, the channel width was narrow, and the navigation speed was fast. Only fixed water depths were simulated in this study; however, it is a fact that the squat effect also increases the intensity of the bank effects. Ship operators can also take advantage of the characteristics of bank effect to help operate ships when turning in channels.

5. REFERENCES

1. ITTC 2010. The Manoeuvring Committee, *Final Report and Recommendations to the 26th ITTC*.
2. LO, D. C., SU, D.T., CHEN, J.M., Application of Computational Fluid Dynamics Simulations to the Analysis of Bank Effects in Restricted Water, *J Navigation, Volume 62, pp 477-491*, 2009.
3. NORRBIN, N.H., Bank Effects on a Ship Moving Through a Short Dredged Channel, *Proceedings 10th Symposium on Naval Hydrodynamics, pp 71–88*, 1974.
4. CH'NG, P.W., An Investigation into the Influence of Bank Effect on Ship Maneuvering and Its Mathematics Modeling for a Ship-Handling Simulator, *ME. Thesis, School of Mechanical and Manufacturing Engineering.the University of New South Wales, Australia*, 1991.
5. CH'NG, P.W., RENILSON, L.J., A Method of Calculating the Ship Bank Interaction Forces and Moments in Restricted Water, *International Shipbuilding Progress*, 1993.
6. LI, D.Q., Experiments on Bank Effects under Extreme Conditions, *SSPA Report, Goteborg, Sweden, No. 113*, 2000.
7. PEDERSEN P.T, Review and Application of Ship Collision and Grounding Analysis Procedures, *Marine Structures, Volume 23, PP 241-262,* 2010.
8. LO, D.C., Numerical Simulation of Hydrodynamic Interaction Produced During the Overtaking and the Head-on Encounter Process of Two Ships, *Engineering Computations, Volume 29, pp 83-101*, 2012.
9. ZHOU M.G, MA S.J and ZOU Z.J, CFD-Based Hydrodynamic Analysis for a Ship Sailing Along a Bank in Restricted Waters, *International Journal Maritime Engineering, Volume 155, Part A2, PP 49-58,* 2013.
10. MA S.J, ZHOU M.G, ZOU Z.J, Hydrodynamic Interaction Among Hull, Rudder and Bank for a Ship Sailing Along a Bank in Restricted Waters, *Journal of Hydrodynamics*, *Volume 25(6), PP 809–817,* 2013.
11. HIRT, C.W., NICHOLS, B.D., Volume of Fluid (VOF) Method for Free Boundaries, *J Comput Phys, Volume 39, pp 201-225,* 1981.
12. WEI, G., A Fixed-Mesh Method for General Moving Objects, *Flow Science, Inc,* 2005.
13. BAHA, M.S., Identification of Finite-Degree-of-Freedom Models for Ship Motions, *Virginia Polytechnic Institute and State University,* 2000.
14. WEI, G., An Implicit Method to Solve Problems of Rigid Body Motion Coupled with Fluid Flow, *Flow Science, Inc,* 2006.

APPENDICES

Table 1 Geometric data of the two types of ship models

Parameters	Ship 1	Ship 2	Unit
Length between perpendiculars (LPP)	230.0	171.0	m
Ship width (*B*)	32.2	28	m
Draft (T)	10.8	9.4	m
Displacement (Δ)	53,330	33,310	tons

Table 2 Comparison of computed and dockyard measured resistances (Wei [14])

Top stream velocity (*m/s*)	5.04	5.88	6.72	7.98
Measured resistance (*N*)*	171.4	178.2	188.2	217.1
Grid1	169.2	182.1	184.3	211.2
Error (%)	1.28	2.19	2.07	2.72
Grid2	170.4	180.2	185.2	213.6
Error (%)	0.58	1.12	1.59	1.61

*Source of measured resistance: Courtesy of the Azimut yacht company

(a) Container ship

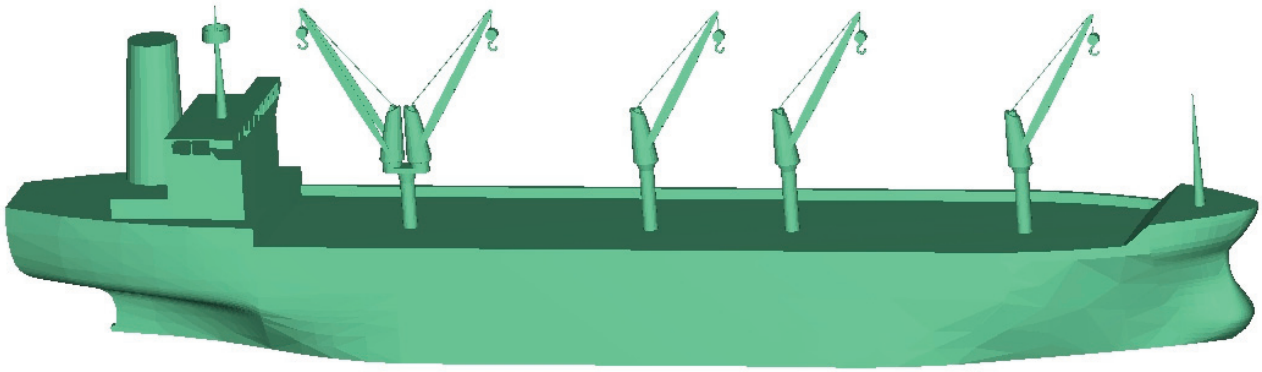

(b) Multipurpose ship

Figure 1. The two types of 3D ship models (a) Ship 1 (container ship) and (b) Ship 2 (multipurpose ship)

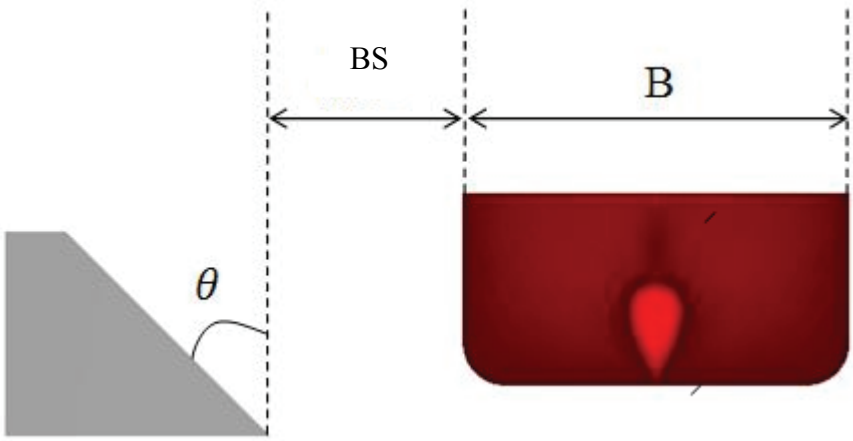

Figure 2. Schematic diagram of bank-to-ship distance (BS) and the bank angle

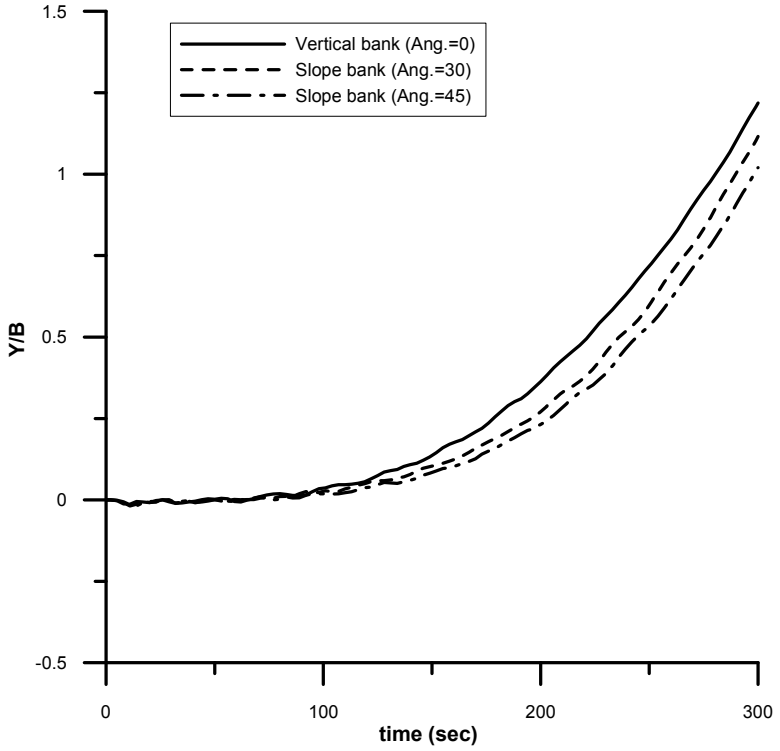

(a) Ship 1

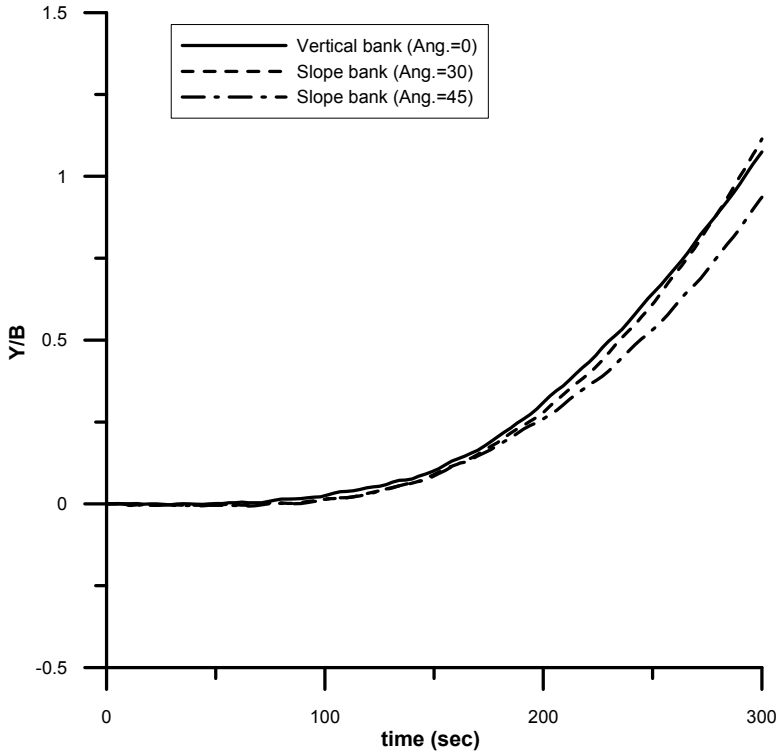

(b) Ship 2

Figure 3. Variance of center of mass deviating from the bank for (a) Ship 1 and (b) Ship 2

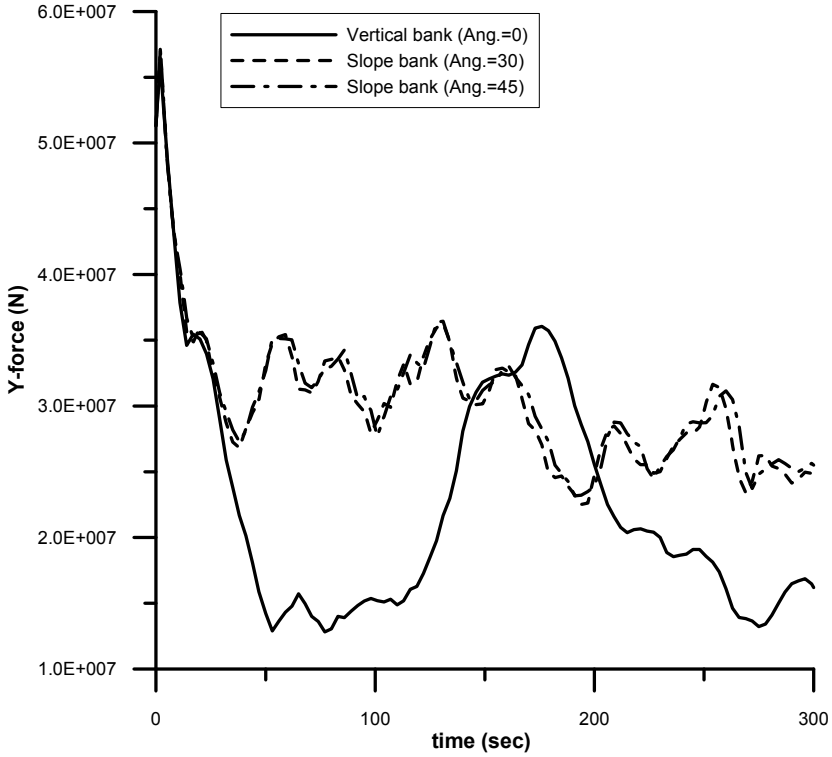

(a) Ship 1

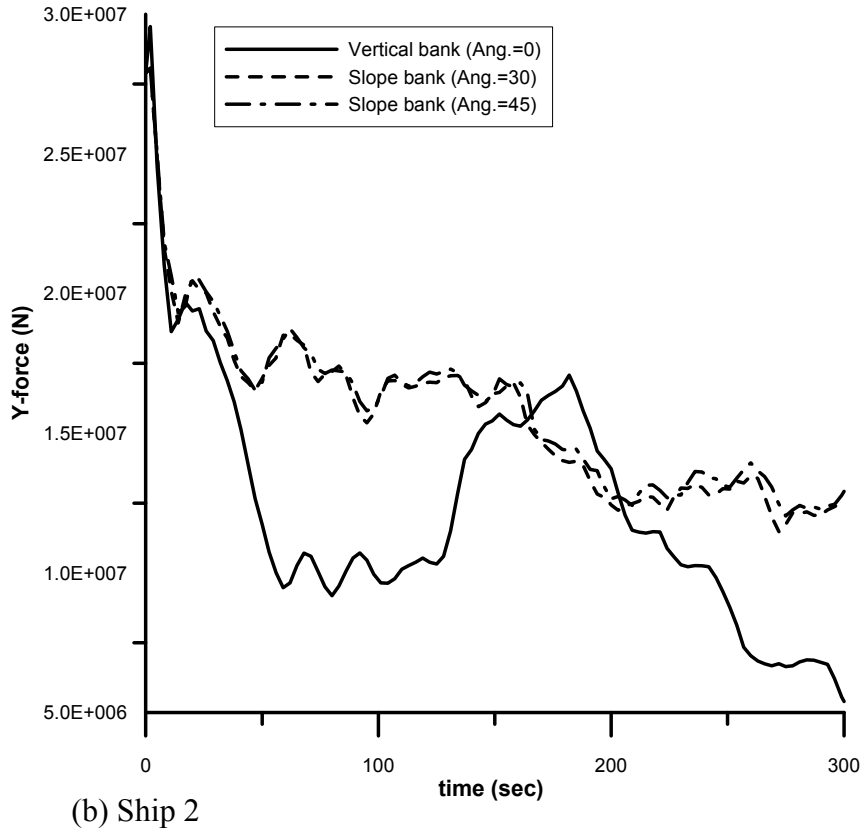

(b) Ship 2

Figure 4. Variance of sway force for (a) Ship 1 and (b) Ship 2

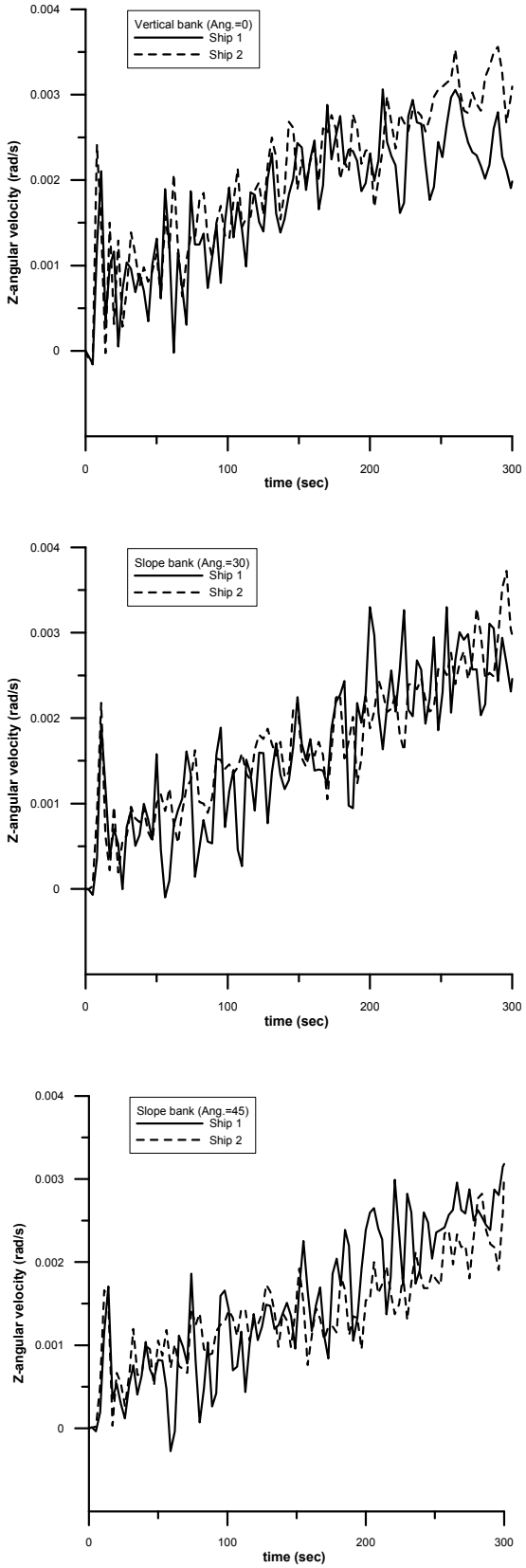

Figure 5. Variance in angular velocity with respect to various bank angles

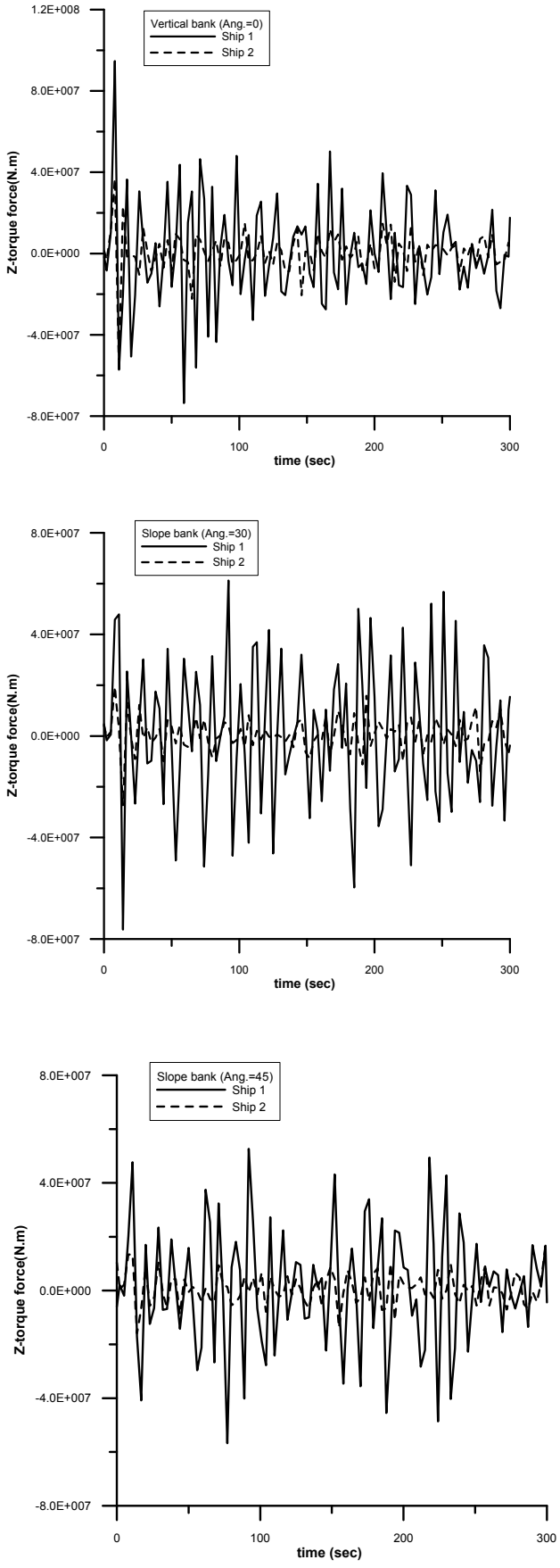

Figure 6. Variance of yaw moment influenced by various bank angles

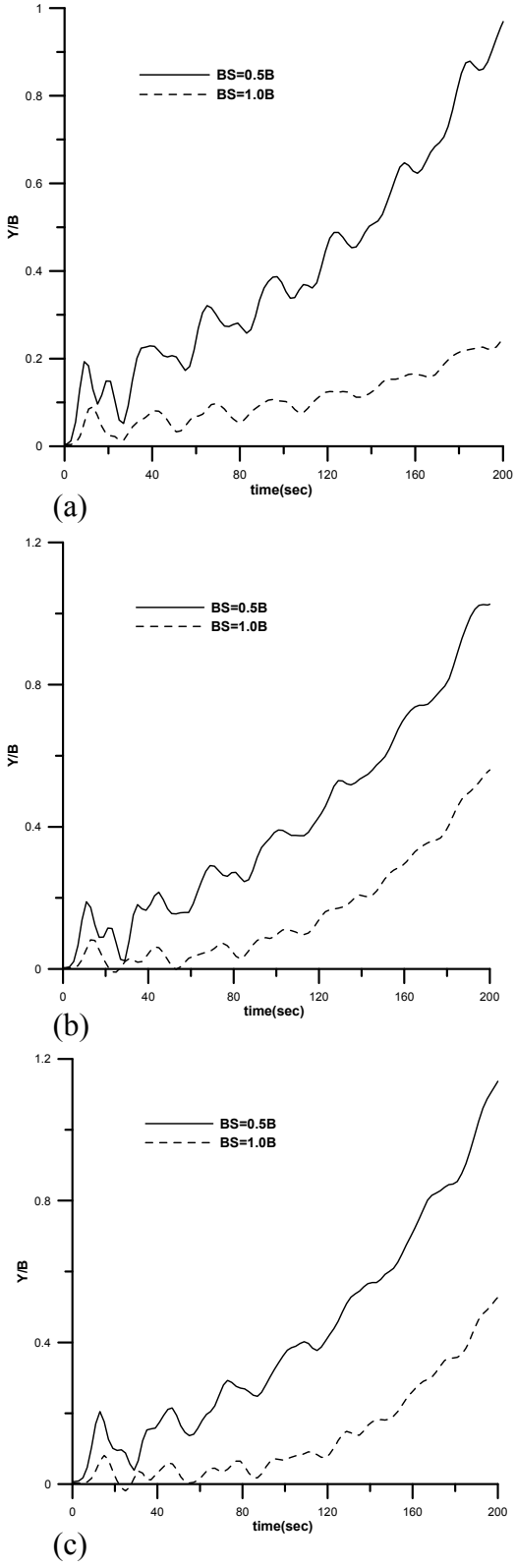

Figure 7. Variance of center of mass deviating from the bank at bank-to-ship distance (0.5B and 1.0 B) for (a) $\theta = 0°$ (b) $\theta = 30°$ (c) $\theta = 45°$

t = 50 s

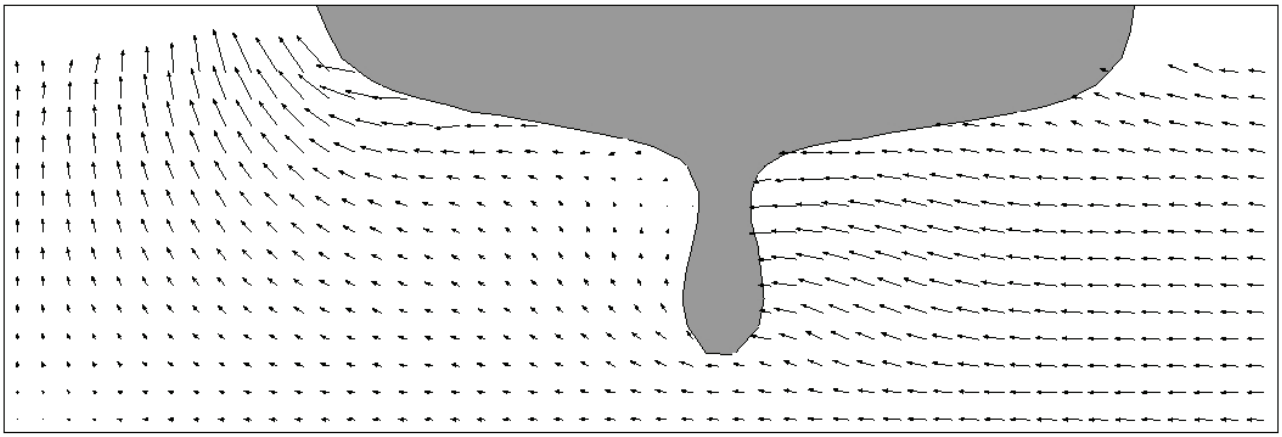

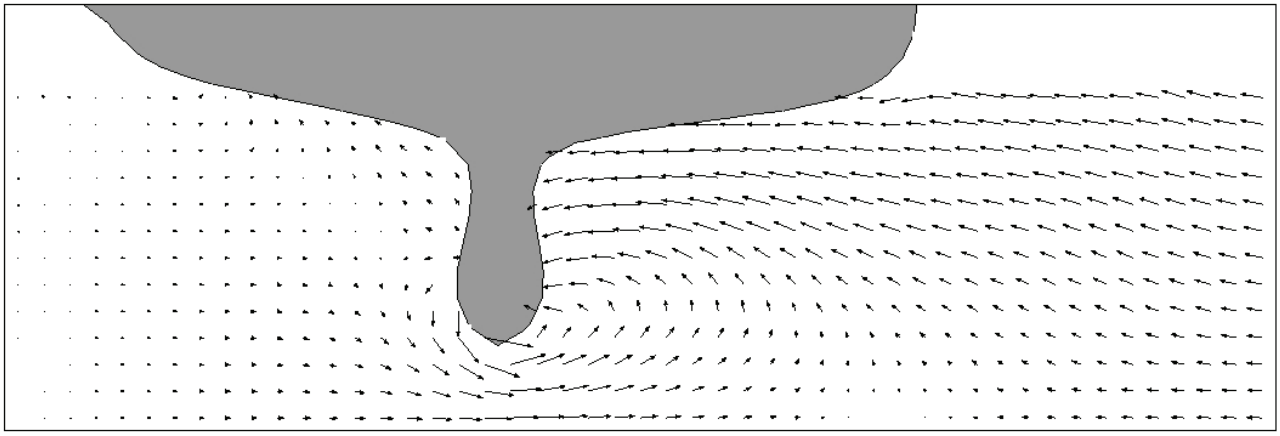

t = 150 s

Figure 8. Stern cross-sectional velocity field

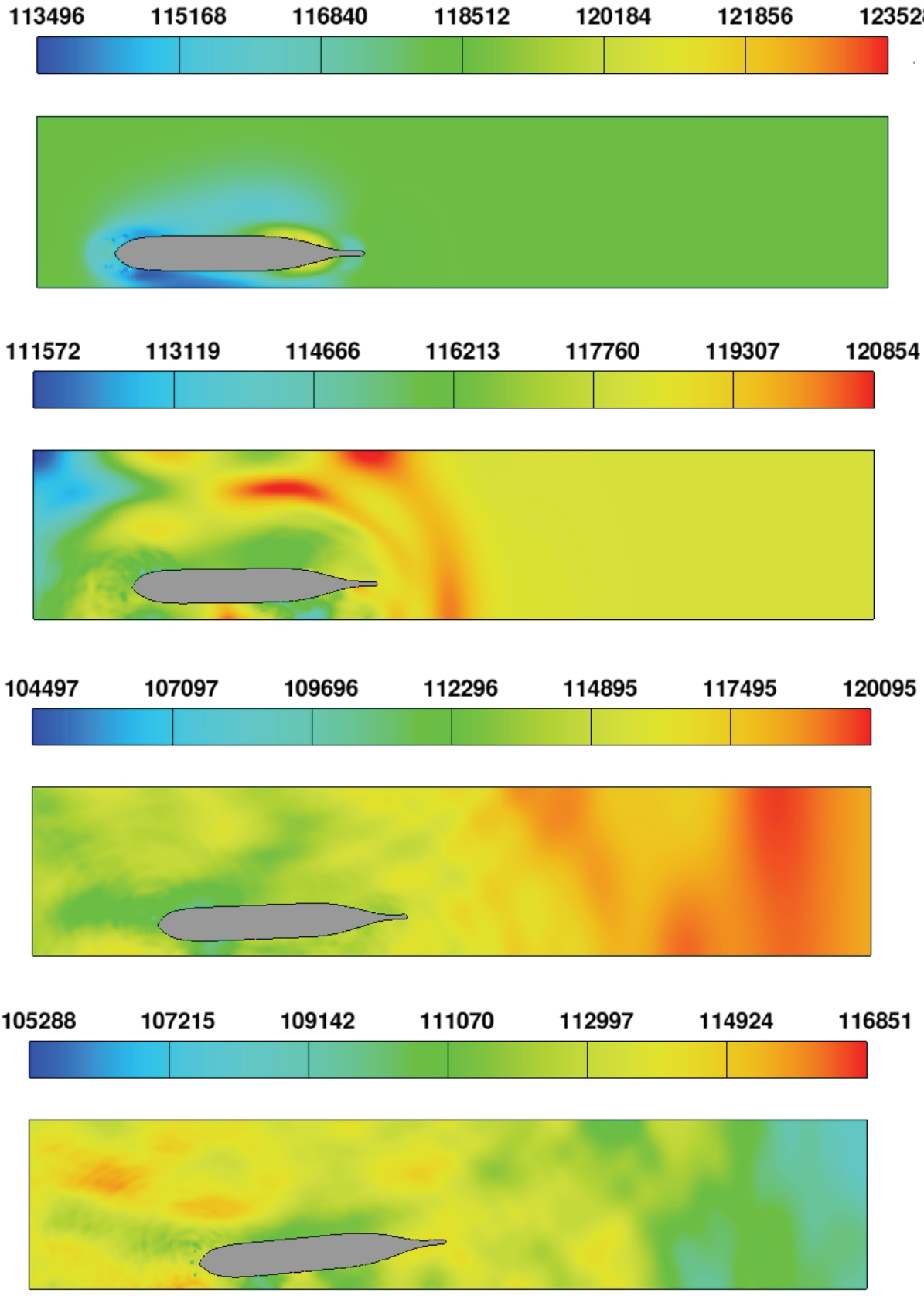

Figure 9. Pressure variation of Ship 1 on the *x-y* plane (from t = 5, 20, 50, to 100 s)

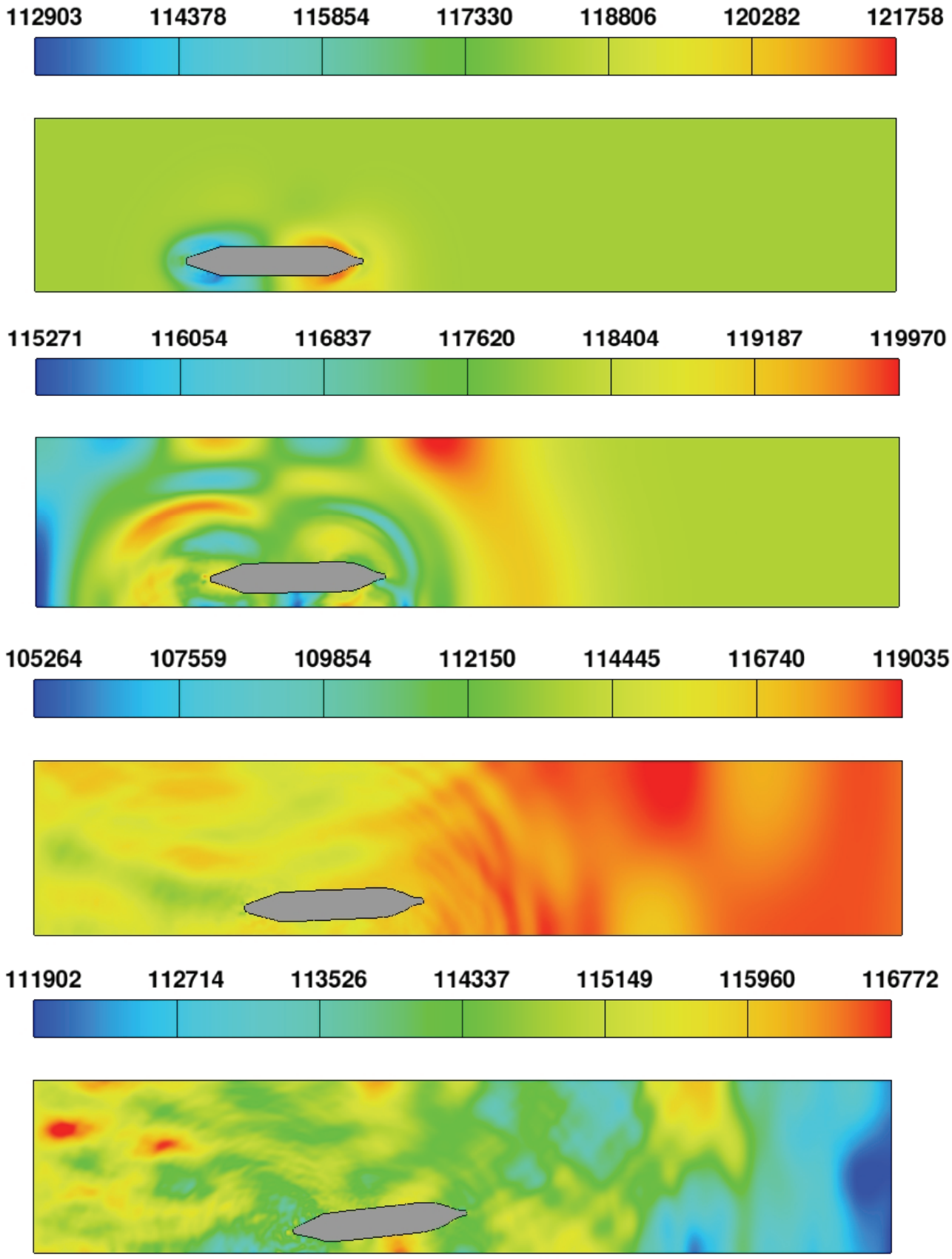

Figure 10. Pressure variation of Ship 2 on the *x-y* plane (from t = 5, 20, 50, to 100 s)